component normal to the surface together with the component tangential to the surface; the latter is unchanged during passage through the shock layer. Note from these figures and Table I that the cutoff points for total drop breakup occur before a drop has been substantially decelerated or deflected.

Conclusions

Drop breakup effects induced by high-speed shock layers must be accounted for in calculating surface damage caused by raindrops. Depending on the flight conditions and vehicle configuration, a large fraction of the entering drop mass may be dissipated in the shock layer, never reaching the vehicle surface. Based on correlations of recent experimental data, including the actual drop mass removal histories, calculations show that both the stripping and catastrophic breakup modes are important in the vehicle stagnation region. In the downstream conical-flow region, on the other hand, the stripping mode of breakup is dominant. In either case, drop breakup is a much more significant mechanism than deceleration or deflection for protecting the surface of a high-speed vehicle from incoming rain.

References

[1] Ranger, A. and Nicholls, J., "Aerodynamic Shattering of Liquid Drops," *AIAA Journal*, Vol. 7, No. 2, Feb. 1969, pp. 285–290.

[2] Waldman, G. D. and Reinecke, W. G., "Particle Trajectories, Heating and Breakup in Hypersonic Shock Layers," *AIAA Journal*, Vol. 9, No. 6, June 1971, pp. 1040–1048.

[3] Nicholson, J., "Drop Breakup by Airstream Impact," *Rain Erosion and Associated Phenomena*, Rept. N68-19401-427, Royal Aeronautical Establishment, Farnborough, England, 1967.

[4] Engel, O. G., "Fragmentation of Waterdrops in the Zone Behind an Air Shock," *Journal of Research of the NBS*, Vol. 60, No. 3, March 1958, pp. 245–280.

[5] Reinecke, W. G. and Waldman, G. D., "A Study of Drop Breakup Behind Strong Shocks with Applications to Flight," AVSD-0110-70-RR, SAMSO-TR-70-142, May 1970, Avco Corp., Wilmington, Mass.

[6] Reinecke, W. G. and Waldman, G. D., "An Investigation of Water Drop Disintegration in the Region Behind Strong Shock Waves," *3rd International Conference on Rain Erosion and Related Phenomena*, Aug. 1970, Hampshire, England.

[7] Reinecke, W. G. and McKay, W. L., "Experiments on Water Drop Breakup Behind Mach 3 to 12 Shocks," AVATD-0172-69-RR, June 1969, Avco Corp., Wilmington, Mass.

[8] Campen, C. F., Jr. et al., eds., *Handbook of Geophysics*, Revised Edition, Macmillan, New York, 1960.

SEPTEMBER 1972 AIAA JOURNAL VOL. 10, NO. 9

Experimental Investigation of Recirculating Cells in Laminar Coaxial Jets

N. R. WARPINSKI,* H. M. NAGIB,† AND Z. LAVAN‡
Illinois Institute of Technology, Chicago, Ill.

Utilizing several means of introducing smoke into the flowfield for careful visualization in addition to hot-wire techniques, the present investigation establishes the existence of recirculating cells on the axis of laminar circular coaxial mixing jets when the outer jet is substantially faster than the inner one. The experiments are performed in a specially designed facility producing laminar flows up to considerably high Reynolds numbers. The characteristics of the cells and the flow conditions that bring them about are documented by smoke photographs in the Reynolds number-velocity ratio plane and the results are compared to previous analytical predictions. Agreement is found between the theoretically predicted incipient cell formation curve and the one obtained experimentally in spite of the observed unsteadiness of some of the cells. The cells are found to fall into three categories with different flow characteristics involving unsteadiness in position, and shear layer instabilities which result in higher mixing with the outer streams. Qualitative agreement is found between the hot-wire mean velocity measurements and the numerical calculations along the axis of the mixing chamber in the presence of cells.

Nomenclature

d = inner jet diameter $= 2r_i$
d_c = diameter of cylinder used in hot-wire calibration
E = hot-wire bridge-top voltage
E_0 = hot-wire bridge-top voltage at zero velocity
f = frequency of cylinder vortex shedding
G = Grashof number
R_c = Reynolds number of cylinder used in hot-wire calibration
Re = Reynolds number based on the total mass flow rate and the outer jet diameter $= 2\overline{W}r/\nu = Re_j(1 + 15\lambda)/4$
Re_j = inner jet Reynolds number $= 2W_i r_i/\nu = 4Re/(1 + 15\lambda)$
r = radial distance measured from the axis of jet
r_i = inner jet radius
r_o = outer jet radius
S = cylinder shedding Strouhal number $= fd_c/U$
U = mean effective velocity measured by hot-wire
W = local mean velocity in the axial direction
$\overline{W}$ = average axial velocity based on the total mass flow rate
W^* = nondimensional local mean velocity in the axial direction $= W/\overline{W}$
W_i = mass flow average axial velocity of inner jet
W_o = mass flow average axial velocity of outer jet
Z = axial distance measured from the exit plane of the inner jet
Z^* = nondimensional axial distance $= Z/r_o$
λ = velocity ratio $= W_o/W_i$
ν = fluid kinematic viscosity

Presented as Paper 72-150 at the AIAA 10th Aerospace Sciences Meeting, San Diego, Calif., January 17–19, 1972; submitted January 25, 1972; revision received April 19, 1972. Supported by NASA Grant NGR 14-004-008 from the Space Nuclear Propulsion Office. The authors would like to thank A. A. Fejer and M. V. Morkovin for the most stimulating discussions during the course of this investigation. The assistance of U. Mehta and K. Bhatt with the numerical calculations is also appreciated.

Index categories: Jets, Wakes, and Viscid-Inviscid Flow Interaction; Nuclear Propulsion.

* Research Assistant, Mechanics and Mechanical and Aerospace Engineering Department; presently at Mechanical Engineering Department, University of Illinois at Urbana. Student Member AIAA.

† Instructor, Mechanics and Mechanical and Aerospace Engineering Department. Associate Member AIAA.

‡ Associate Professor, Mechanics and Mechanical and Aerospace Engineering Department. Member AIAA.

Introduction

THE mixing of confined coaxial jets has many applications (e.g., jet pumps, thrust augmentors, and ejectors) and has

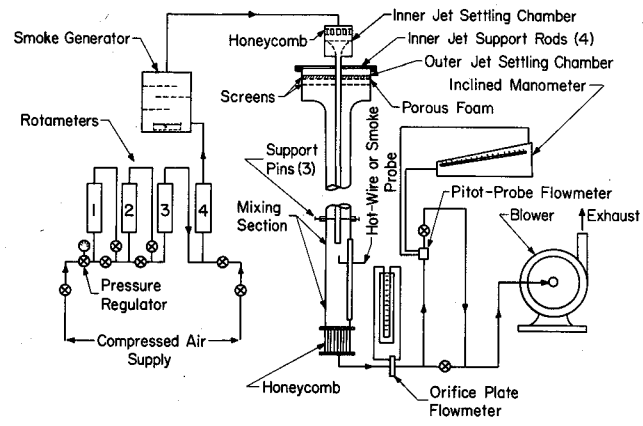

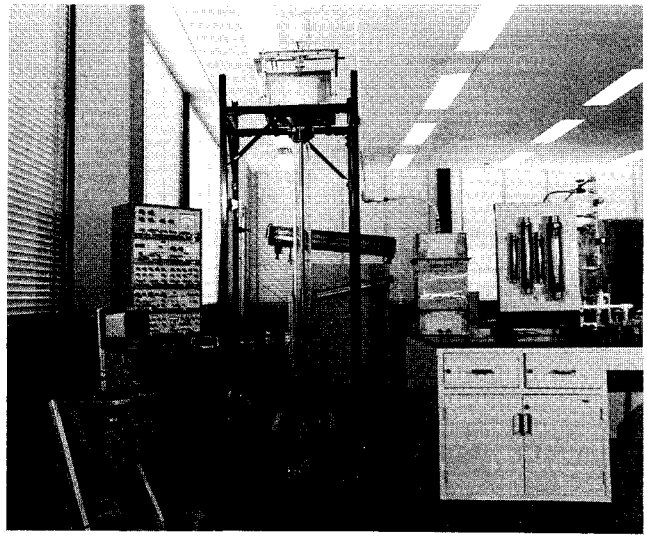

Fig. 1 Schematic diagram and photograph of experimental apparatus.

been recently studied by a number of investigators. The first extensive study of the *laminar* mixing of confined jets was carried out by Wood,[1] who showed experimentally that under certain conditions the flow in the mixing region remains laminar. The analytical and experimental work of Shavit and Lavan[2-4] has been motivated by the concept of a coaxial gaseous fuel nuclear rocket engine. This concept requires minimum mixing between the heavy, slow-moving fuel jet and the light, fast-moving outer propellant jet. In the analytical phase of their studies, numerical techniques were used to obtain solutions of the *steady* Navier-Stokes equations. In these solutions recirculating cells were detected along the axis of the jets just downstream of the exit of the inner jet. These cells were predicted to occur at high-velocity ratios λ and the incipient cell formation curve (i.e., the flow conditions under which the cells are just formed) was found to depend on the radius ratio (see Fig. 5 of Ref. 2).

In the experimental phase of their study, Shavit and Lavan[2-4] determined the conditions under which the flow in the mixing region is laminar for both Air-Air and Argon-Air mixing jet systems. The boundary of the laminar flow regime was found to be correlated for both systems when plotted in the mass flux ratio vs an effective jet Reynolds number plane (see Fig. 13 of Ref. 3). Their measurements of mean velocity profiles along the mixing chamber showed excellent agreement with the calculated profiles when the measured initial mean velocity profile at the exit plane of the inner jet was used as the upstream boundary condition for the numerical computations.

Using shadowgraph visualization Rozenman and Weinstein[5] observed recirculating cells along the axis of a confined *turbulent* jet. Their data show that the recirculating region is formed at velocity ratios λ higher than 13 for homogeneous jets and higher than 26 for heterogeneous jets (Freon 12-Air).

The present study is an experimental verification of the findings of Shavit and Lavan[2,4] regarding the recirculating cells and is concerned with the characteristics of such cells and the flow conditions that bring them about. The experiments utilize smoke visualization and quantitative hot-wire techniques in a specially designed facility in which laminar flow can be sustained up to high Reynolds numbers.

Facility and Instrumentation

A. Apparatus

A schematic diagram and a photograph of the apparatus are shown in Fig. 1. (For a detailed description of the apparatus, see Ref. 6). The apparatus, which was originally designed and constructed by Shavit,[4] is modified for the use in the present investigation. The outer plexiglas tube (approx. 4 in. i.d.) and the inner stainless-steel tube (approx. 1 in. i.d.) are supported vertically and have a mixing chamber 30 in. long (radius ratio = 0.25). Both tubes are sufficiently long to yield fully developed laminar velocity profiles at the exit plane of the inner jet. Compressed air is blown through the inner tube to the mixing section and ambient air is drawn through the outer tube into the mixing region by a blower situated downstream of the test section. Both streams mix in the test section and are drawn out by the blower and exhausted into the room.

The stainless-steel inner jet tube is 67 in. long with the three inches at the exit tapering in wall thickness to 0.008 in. $\pm$ 0.001 in. The flow control for the inner jet is shown schematically in Fig. 1. Rotameters are chosen for this study to permit continuous monitoring of the flow rate and to detect any low frequency fluctuations in the operating flow rate. All rotameters were carefully calibrated for the purpose of the present study.

Smoke may be introduced into the inner jet flow as it passes through the smoke generator (see Fig. 1) by heating kerosene in a pyrex tray with two heater coils. The coils are connected in series to a powerstat which can be used to control the amount of kerosene smoke added to the flow entering the inner jet.

The contraction section connecting the settling chamber to the outer jet provides a separation free flow and a uniform velocity profile at the entrance to the outer tube. A slot equipped with a traversing mechanism which is capable of traversing the probes in both the axial and radial directions is used for hot-wire measurements and local smoke injection. For accurate positioning, and to eliminate vibrations, the inner tube is supported by three needles, 120° apart and 10 in. upstream of its exit. The size of the needles (0.032 in. diameter, 2 in. long) is chosen in order not to disturb the flow (for details see Ref. 4).

B. Visualization Techniques

Two means of introducing smoke into the flowfield for careful visualization are utilized in the present study. To determine the Laminar-Transition boundaries and to visually monitor the hot-wire studies, the smoke generator described above is utilized to mix a controlled amount of smoke into the inner jet stream. High-intensity lamps are focused on the mixing region so that only small amounts of smoke are required for visualization and the variations in density and temperature of the flow are negligible. Care in positioning the high-intensity lights and intermittent operation of the experiments resulted in avoiding the heating of the flowfield and test section by the high-intensity lights.

To visualize the cells, an "L"-shaped hypodermic probe (0.083 in. o.d.) was constructed to inject the smoke locally through the traversing mechanism. The exit of the probe is normally located from $3d$ to $10d$ downstream of the jet exit. Cigar smoke is blown upstream through the probe until the region immediately downstream of the jet exit is sufficiently marked with smoke. When the flow reestablishes its steady state conditions the flowfield is photographed. To take the photographs, the light from a high-intensity strobe (triggered by the camera) is passed through

a thin slit so that only the plane passing through the axis of the tube and parallel to the plane of the film is illuminated.

C. Hot-Wire Calibration

Hot-wires are used in the present study to measure the local mean velocity in the neighborhood of the cell. DISA 55D system anemometer units and associated intrumentation are utilized with specially constructed hot-wire probes. These probes are shaped in order to minimize the aerodynamic disturbances associated with them. This is particularly important in complex flowfields involving reversed flows such as the one present in the cell region. The probe specifications are: stem diameter = 0.155 in., prong length = 1.375 in., prong diameter at stem = 0.025 in., prong diameter at tip = 0.015 in. (tapered prong), prong spacing = 0.125 in., wire diameter = 0.00015 in. (tungsten), sensitive wire length = 0.1 in. (l/d = 670), and the probe angle to the positive Z direction = 60°. For all measurements reported here the wire is oriented in the horizontal direction.

According to the recent measurements of Comte-Bellot et al.[7] the probes used in the present study should have minimum disturbances on the flowfield. A reduced level of perturbation of approximately 2.5% in absolute value is reported for a similar probe. This level of perturbation is found to be almost equal for flows in the positive or negative Z direction for the probe angle used in the present experiments. Smoke visualization is used to indicate the effect on the flowfield due to the presence of the probe near or inside the recirculating cell. No disturbance is observed in this flowfield despite the fact that the presence of hot-wires is known to disturb other recirculating regions (e.g., horseshoe vortices upstream of an obstacle in a laminar boundary layer).

Because of the low velocities present for the flow conditions under consideration, a special probe calibration procedure is required. Calibrating hot-wire probes in a uniform freestream by using a Pitot-probe to obtain the velocity is the most common practice to date. Such a procedure is limited by the minimum Reynolds number at which a Pitot-probe can be operated accurately and the accuracy of measuring small pressure differences.

Roshko's[8] results relating the frequency of vortex shedding behind long, circular cylinders to the mean freestream velocity may be used to measure mean velocities of uniform streams. Stable vortex streets in the range of cylinder Reynolds numbers, R_c, from 50 to 150 are found to be most accurate to determine the mean velocity. The best fit to Roshko's experimental data is

$$S = 0.212(1 - 21.2/R_c), \quad \text{for} \quad 50 < R_c < 150$$

A special calibration tunnel (3 in. test section) having a low level of freestream turbulence (less than 0.1%) and a uniform mean velocity profile, is utilized to calibrate the probes used in this study over the range from 1 to 12 fps. One of several cylinders (0.020 in. $< d_c <$ 0.125 *in.*) is placed in the test section of the calibration tunnel to produce the vortex street. The change in velocity due to the blockage of the cylinders is found to be negligible. Maximum standard deviation of 4% is found during the course of the present study for different cylinder sizes.

The hot-wire probe is first placed in the vortex street and the frequency of shedding is measured by an electronic counter (HP 5233L digital counter). The position of the wire is maneuvered to obtain the maximum output of the velocity fluctuation from one side of the vortex street. The probe is then moved to one side of the cylinder and upstream of it to record the mean freestream velocity.

In order to use the cylinder shedding to calibrate the probes at velocities smaller than 1 fps, cylinders larger than 0.125 in. in diameter are required. The blockage of the flow in the calibration tunnel test section made these measurements inaccurate.

Wygnanski and Champagne[9] conclude that the mean velocity distribution in fully developed pipe flow is truly parabolic as long as no turbulent slugs are present. (Reynolds numbers smaller than approximately 1500.) Therefore, by measuring the flow rate through long circular pipes while the hot-wire is placed on the axis of the pipe near its exit, the probe can be calibrated in the range of velocities below 1 fps.

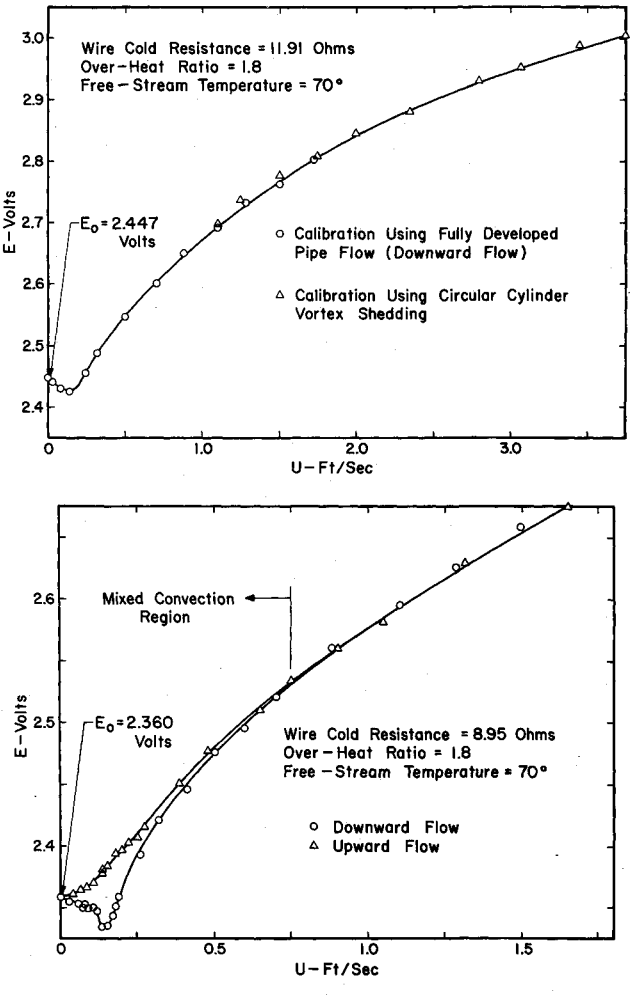

Fig. 2 Typical hot-wire calibration curves.

The influence of free convection on the operation of hot-wires must be accounted for at low velocities. Since the mean flow direction in the present study is downward and the presence of the recirculating cells results in reversed flows, calibration of the wire for both the flow magnitude and direction is required in the mixed convection region of the wire. Calibrating the wire for all velocity directions becomes a very complex procedure. Fortunately, only upward and downward flow directions are present along the axis of the jet, even in the presence of the recirculating cells, due to the axial symmetry.

A pipe (0.82 in. i.d., 8.5 ft long) is used to produce fully developed laminar flow in the upward direction. The flow rate through the pipe is measured by the rotameters discussed in the description of the apparatus. The wire is positioned in the center of the pipe using an indexing head of a milling machine. After calibrating the wire in this configuration, the mean velocity profile in the pipe was measured and excellent agreement with the parabolic distribution was found. The same procedure is repeated for downward flow, while the probe is inside the jet mixing apparatus utilizing the inner jet to produce the fully developed laminar pipe flow. For both upward and downward flow calibration, the hot-wire is placed upstream of the exit of the pipe to minimize the downstream disturbances.

Typical calibration curves of two different hot-wires are shown in Fig. 2. The probes are always operated with the wire in the horizontal direction to avoid the problems introduced by the presence of the prongs on the mixed convection. The top curve shows the agreement between the two methods of calibration in the range where they overlap. The detailed calibration curves of the mixed convection region are shown in the bottom curve of Fig. 2. Although different overheat ratios were tried, the value of 1.8 was found to be adequate for the probes used. To obtain accurate results when using the probes, the values of the free-

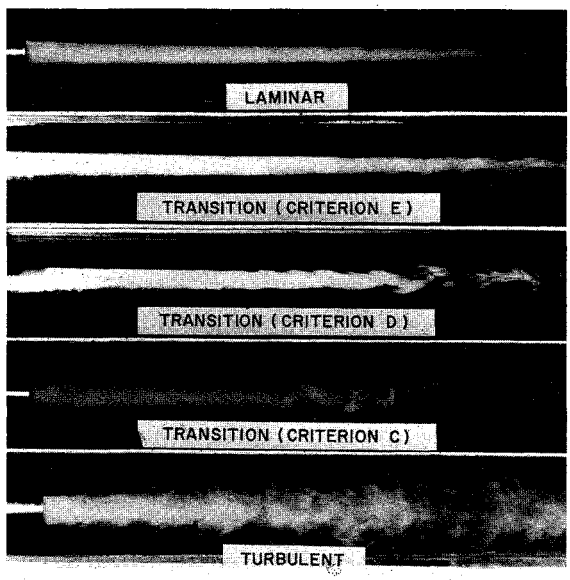

Fig. 3 Smoke visualization for determining laminar-transition-turbulent flow regimes.

stream temperature, the over-heat ratio, and E_o must be exactly the same as the ones recorded during the calibration of the wires.

An interesting side result which can be obtained from the calibration curves presented in Fig. 2 is the condition which separates the mixed and forced convection regions of the operation of hot-wires. Based on an order of magnitude analysis, several heat-transfer texts conclude a value for (G/R_c^2) at this condition to be of the order of one (e.g., see Gebhart,[10] p. 389). However, Gebhart[10] (pp. 394–395) presents experimental evidence which is not in agreement with the order-of-magnitude analysis. On the other hand, he does not give a value for (G/R_c^2) which correlates the data.

At the value of the mean velocity separating the mixed and forced convection regions obtained in the present study (approx. $U = 0.75$ fps), (G/R_c^2) is found to be equal to 0.55×10^{-3} and a value of $E/E_o = 1.08$. From Collis and Williams'[11] data for long wires in a uniform air stream, a value of $(G/R_c^2) = 3.5 \times 10^{-3}$ is estimated. Goodman's[12] results, using conical hot-films in water, yield a value for $(G/R_c^2) = 1.6 \times 10^{-3}$. Recently Hollasch and Gebhart[13] obtained a value for $E/E_o = 1.12$ for the boundary between the mixed and forced convection region from their measurements of hot-wires in water. Rasmussen's[14] data yield a value of $E/E_o = 1.02$ for hot-wires in air. The agreement between the present measurements and the various investigations referenced here confirms the value of these measurements and points to a good practical criterion for the lower boundary on the operation of hot-wires and hot-films in standard applications within the forced convection region to be: *E approximately 15% larger than E_o or that $(G/R_c^2) \approx 10^{-3}$.*

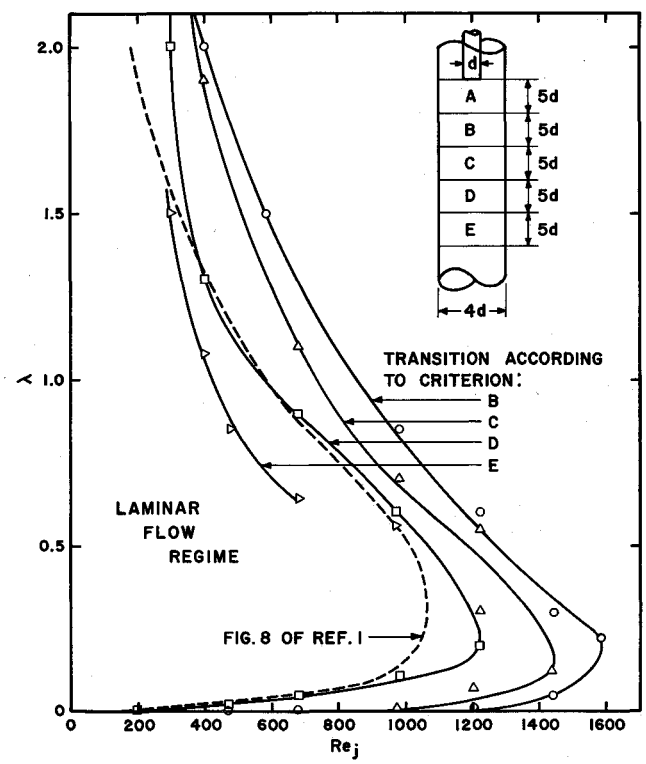

Fig. 4 Dependence of the boundary of laminar flow regime (initiation of transition) on the downstream distance shown in the jet Reynolds number vs velocity ratio plane.

Results

A. Determination of Boundaries of Laminar Flow Regime

In order to establish the conditions under which the flow in the mixing chamber is laminar, smoke is introduced into the inner flow stream. In Fig. 3 five photographs of the resulting smoke patterns are presented. Only the inner jet can be seen here (the outer jet is four times larger) and the lines near the border of the photographs are light reflections. Figure 4 shows the mixing chamber schematically divided into Regions A–E, each covering an axial distance of $5d$ starting from the exit of the inner jet. The flow conditions at which the shear layer between the jets becomes unstable in a specified region are plotted for each region as a function of the jet Reynolds number, Re_j [where $Re = Re_j(1 + 15\lambda)/4$], and the velocity ratio (e.g., a flow condition which becomes unstable at $Z/d = 13$ is considered transitional flow according to criterion C). The A–E criteria were used rather than an exact Z/d criterion because the regular instability shown in the photographs is unsteady in space and tends to fluctuate back and forth along the Z direction. For Re greater than 3200, the flow in the mixing chamber is found not to be laminar at all velocity ratios. Checks using hot-wires agree with the visualization results and confirm that the outer stream is also laminar when the inner stream and shear layer are laminar.

The theoretical calculations of Shavit and Lavan[2,4] show that the size and location of the cell is always limited to less than three inside jet diameters downstream of the jet exit plane. Flow disturbances due to transition to turbulence that occur at distances larger than $5d$ are believed to be, therefore, of negligible effect on the presence of recirculating cells under laminar flow conditions. Flow conditions limited by curve B of Fig. 4 are adequate to study the recirculating cells under laminar flow conditions. Data at higher velocity ratios is obtained, but is shown only for curve B at the top of Fig. 5. A similar curve for the region immediately downstream of E which was obtained by Shavit and Lavan[2–4] using hot-wires is also included in Fig. 4. Despite a slight difference in their apparatus, the agreement with their results can be noted in this figure.

B. Flow Visualization Results

Figure 5 shows both the experimental and numerical incipient cell formation results (i.e., flow conditions under which the cells are just formed) in the Reynolds number versus velocity ratio plane. While at low velocity ratios cells are not observed, at high velocity ratios the presence of recirculating cells is predicted theoretically and confirmed experimentally. The theoretical curve labeled "Original Numerical Results" is the curve obtained by Shavit and Lavan[2,4] for the same radius ratio as in the present study (0.25). Although a stretching transformation in the axial direction was used in obtaining their results, a uniform grid distribution was used in the radial direction.

The theoretical curve labeled "Improved Numerical Results" is obtained during the course of the present investigation using the computer program of Bhatt[15] (an extension of Shavit and

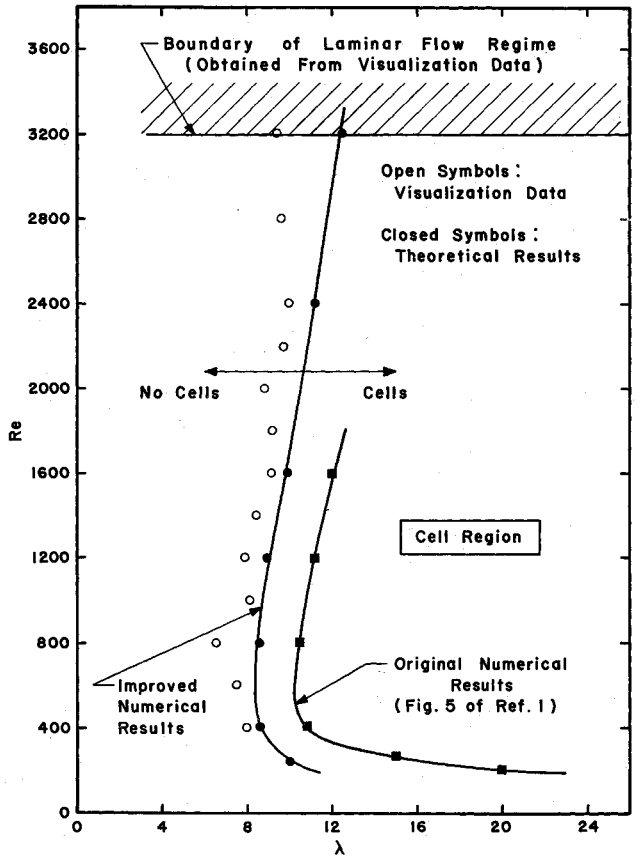

Fig. 5 Incipient cell formation curve plotted in the Reynolds number vs velocity ratio plane.

Lavan's[2,4] work) with the addition of a stretching transformation in the radial direction and a much larger number of grid points. This modification in the numerical procedure was motivated by the experimental observations of recirculating cells much smaller than the smallest cells predicted by Shavit and Lavan.[2,4] When the size of these cells is compared to the original grid size, the conclusion was reached that the original grid size is inadequate to detect the "true" incipient cell formation curve. This is particularly true for small radius ratios since the extent of the recirculating region in the radial direction is found to be always equal to or smaller than the size of the inner jet. Several grid points within the recirculating region are required in order to predict the cell accurately. The transformation in the radial direction which was incorporated into the program is given by:

$$r/r_o = C \tan(D\xi)$$

where ξ is the transformed nondimensional radial coordinate. C and D are constants which depend on r_o/r_i and ξ_i. They are determined from the following expressions:

$$\tan D - (r_o/r_i) \tan(D\xi_i) = 0$$

and

$$C = 1/\tan D$$

The value of $\xi_i = 0.5$ is used to obtain the present results. This choice of ξ_i distributes the grid points equally between the inner and outer jets. The same transformation in the axial direction which was used by Shavit and Lavan[2-4] is employed in obtaining the present results. The present curve is obtained by running the program on a UNIVAC 1108 computer at various constant Reynolds numbers for different velocity ratios in the neighborhood of the flow conditions where the curve is found from the experimental results. The number of grids used for all runs is 60 in the axial direction and 37 in the radial direction. The upstream boundary condition (fully developed flow in inner and outer jets) is located at $Z = -r_o$ and the transformation in the axial direction places 11 grid points from $Z = -r_o$ to $Z = 0$ and the same number of points from $Z = 0$ to $Z = r_o$. The closed circles shown in Fig. 5 are the flow conditions between those where a cell is predicted and those where a cell is not predicted (e.g., at $Re = 1200$, no cell at $\lambda = 8.75$ and a cell at $\lambda = 9$). When a yet finer grid is employed in the program for the case of $Re = 1200$, the shift in the curve is found to be within the scatter of the Improved Numerical Results. It is therefore believed that the incipient cell formation curve obtained from the Improved Numerical Results represents the occurrence of the physical phenomenon and is an accurate solution of the steady Navier-Stokes equations.

The line bounding the hatched region in the top of Fig. 5 represents the boundary of the laminar flow regime which is discussed in the previous section and is labeled curve B in Fig. 4. For $Re < 3200$ and $\lambda > 4$, the flow in the mixing chamber for at least $5d$ downstream of the jet exit plane is found to be laminar. It should be noted here, however, that cells can also be observed at high Reynolds numbers (i.e., under turbulent flow conditions); the results of the present investigation are only limited to the presence of cells under laminar mixing conditions.

The experimental results shown in Fig. 5 are obtained using local smoke injection. These points are obtained at different fixed Reynolds numbers by varying the velocity ratio. A cell is first detected at large velocity ratio λ and as λ is slowly decreased the cell becomes smaller and moves downstream. The incipient cell formation location is defined as the flow condition where the smoke marking the region downstream of the jet exit moves downward along the axis of the jet, decelerates to a stop (at a position approximately $2d$ downstream of the exit of the jet), and then continues downward without reversing direction. At slightly smaller velocity ratios λ the smoke marking the flow along the axis decelerates as it moves downstream, maintains a finite velocity and then accelerates. The probe is occasionally moved far downstream after the smoke is blown upward to determine if it has any effect on the incipient cell formation curve. The difficulties involved in obtaining quantitative data from flow visualization techniques are well known. In the present investigation most of the flow visualization techniques' parameters that may effect the results are carefully regulated to minimize these difficulties (e.g., the various means of introducing the smoke into the flowfield, the photographic techniques and the amount of

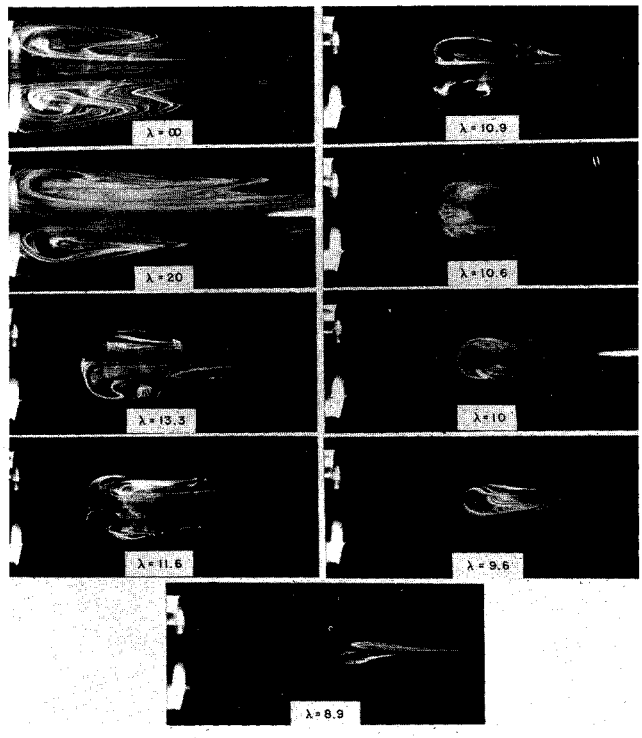

Fig. 6 Sequence of smoke visualization of cells at constant Reynolds number ($Re = 1200$) for decreasing velocity ratios.

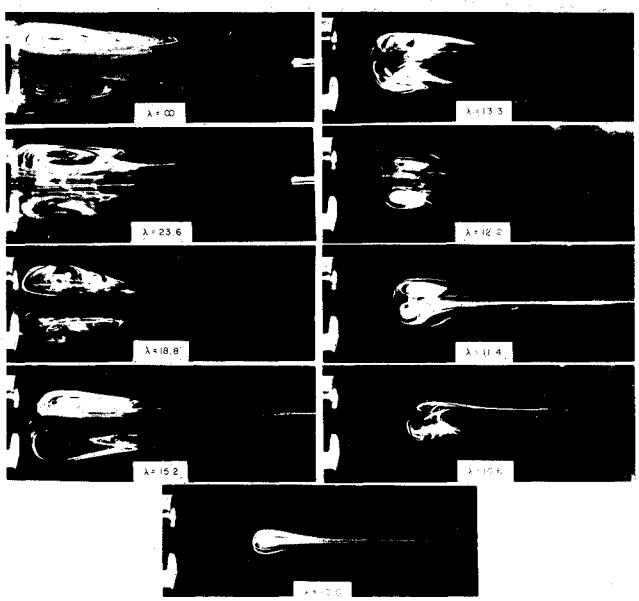

Fig. 7 Sequence of smoke visualization of cells at constant Reynolds number (Re = 1600) for decreasing velocity ratios.

smoke and the manner by which the smoke is introduced into the flowfield); see section on Visualization Techniques. It is therefore believed that the accuracy of the visualization data shown in Fig. 5 is within the scatter of the experimental points. The inaccuracy in the flow rate measurements (in both Re_j and Re) in obtaining the incipient cell formation curve at $Re < 400$ prevented the collection of sufficiently reliable data in this range.

Sequences of photographs showing the cells at two fixed Reynolds numbers (1200, 1600) and decreasing velocity ratios are shown in Figs. 6 and 7. All cells shown in Figs. 6–8 are two-dimensional photographs recorded using a plane sheet of light passing through the axis of the mixing region. (Only the inner jet can be seen in these photographs; the outer jet is four times larger.) In some of the photographs of Fig. 6 the upstream tip of the smoke probe can also be seen positioned near the axis of the jet at $Z \approx 3d$. Figure 8 shows a sequence at a fixed velocity ratio

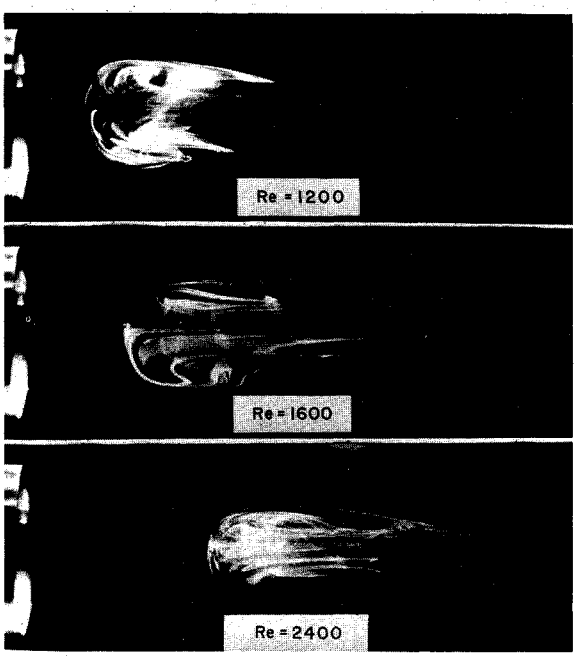

Fig. 8 Sequence of smoke visualization of cells at constant velocity ratio (λ = 13.3) for increasing Reynolds numbers.

(13.3) and three different Reynolds numbers. As seen in Figs. 6–8 the cells are found to be smallest and located farthest downstream from the jet exit when the operating flow conditions are close to the incipient formation curve. At these conditions the recirculation within the cells is observed to be very slow and the diffusion to the surrounding stream is small. When these cells are marked with smoke they can be observed for long periods of time (e.g., 10 min).

At flow conditions far from the incipient curve, the photographs show that the cells increase in size and approach the jet exit plane. At very large velocity ratios ($\lambda \to \infty$) the cell is observed to be located partially inside the inner jet (i.e., the upstream stagnation point is located upstream of the jet exit plane). The velocities within these cells are higher, as is the diffusion rate, and the cells can be observed only for a short duration of time. Most photographs show a smoke tail downstream of the cells. This smoke tail marks the flow which is diffused out from the recirculating region to the surrounding stream and is convected downstream along the axis of the mixing region.

When the cells are immediately downstream of the exit plane of the jet, they are observed to be unsteady in position and tend to oscillate in oblique angles with respect to the axis of the jet. As seen in Figs. 6 and 7, the location of the downstream stagnation point of the cells remains approximately in the same axial position independent of the velocity ratio for a given Reynolds number.

When the upstream stagnation point of the cell is upstream or immediately downstream of the exit plane ($Z/d < 1$) a shear layer instability occurs which can be clearly seen, for example, in Fig. 7 for $\lambda = \infty$. This instability is believed to be due to the high velocity gradient in the radial direction existing under these conditions. This instability is often observed to amplify into a vortex ringlike region which the surrounding stream ejects downstream. This results in opening the originally closed recirculating region and decreasing the size of the cell. The consequent entrainment of the surrounding stream into the recirculating region and the reestablishment of the instability is observed. This relaxation-type phenomenon occurs periodically. This phenomenon causes the downstream stagnation point of the cell to be unsteady in its location (also confirmed by hot-wire measurements).

C. Hot-Wire Results

Using the hot-wire probe described earlier and utilizing calibration curves such as the ones shown in Fig. 2, the mean velocities in the neighborhood of the recirculating cells are found to include the mixed convection range of the hot-wire. As discussed in the hot-wire calibration section, knowledge of the direction of the mean velocity is required in order to accurately determine the velocity in this range. Because of the axial symmetry the

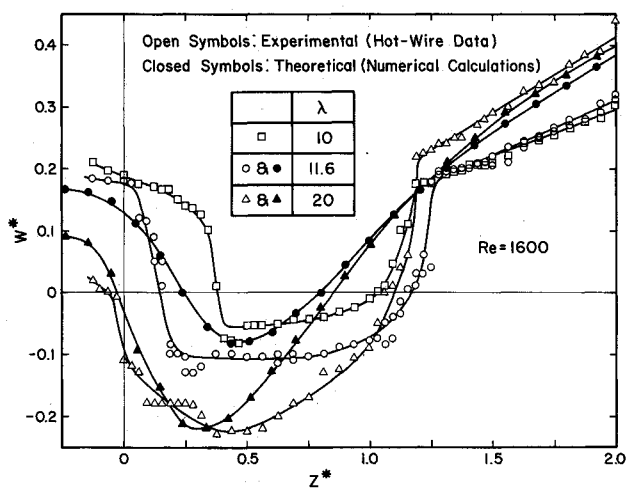

Fig. 9 Hot-wire measurements and numerical calculations of the mean axial velocity along centerline at constant Reynolds number (Re = 1600) for different velocity ratios.

velocity along the axis of the mixing chamber is either in the positive or negative Z direction. Single horizontal wires calibrated as outlined above can, therefore, be used to measure the mean velocity along the axis of the jets.

Figure 9 shows mean axial velocity distributions along the centerline of the mixing chamber for three different velocity ratios at the same Reynolds number ($Re = 1600$). The results of the numerical calculations, using the same computer program described above, for two of the velocity ratios and the same Reynolds number are also shown. In this figure the cells are represented by the portion of the curves with negative velocities. Long time averages (approx. 1 min) are used to record the hot-wire bridge output.

The hot-wire was first located along the axis of the inner jet and upstream of its exit plane. Traversing the probe in the positive Z direction, the mean velocity is recorded based on the lower branch of the calibration curve (similar to that in Fig. 2). The bridge voltage is first observed to decrease to a minimum and then increase until it reaches the value E_o at the upstream stagnation point of the cell. Further traversing of the probe results in increasing bridge voltages along the upper branch of the calibration curve to a maximum negative velocity. Subsequently decreasing values on the same branch are recorded until the downstream stagnation point is reached ($E = E_o$). Downstream from the downstream stagnation point, the lower branch of the calibration curve is utilized once more. It should be pointed out that due to the complexity of accurately obtaining these measurements in the mixed convection region of the hot-wire, the curves presented here are only indicative of trends and magnitudes of the mean velocity and are not of precise quantitative value. The measurements near the downstream stagnation point incorporate further inaccuracy due to the unsteadiness of the flow in this region which is discussed in the visualization section and can be observed on oscilloscope traces.

Conclusions

1) Agreement is found between the theoretically predicted incipient cell formation curve and the one obtained experimentally (Fig. 5) in spite of the observed unsteadiness of some of the cells. The cells observed near the incipient formation curve are the most stable, which may account for the good agreement with the theoretical results of the *steady* Navier-Stokes equations. The divergence between the theoretical and experimental results at high Reynolds numbers, Re, may be attributed to the influence of the turbulence on the experimental results (near the boundary of laminar flow as shown in Fig. 5) and the influence of large Reynolds numbers on the convergence of the numerical calculations.

2) The observed cells seem to fall into three categories. a) At high Reynolds numbers, when the cell is partially inside the inner jet, it is observed to be stationary in space and shear layer instabilities are observed along its boundaries. These instabilities result in higher mixing between the fluid in the cell and the outer stream. As seen from the hot-wire results the velocities are much higher within these cells than in cells situated farther downstream. b) When the upstream stagnation point of the cell is just downstream of the jet exit plane, the cell is observed to be somewhat unstable in its position resulting in instantaneous oblique but symmetric cells. No shear layer instability is observed. c) Cells that are located far downstream are found to be the most stable in space and time. The velocities within these cells are observed and measured to be much smaller than the velocities within the cells that are located farther upstream.

3) The visualization and hot-wire results confirm the trends in the characteristics of the cells as a function of Re and λ that are predicted by the numerical results.

4) Qualitative agreement is found between the hot-wire mean velocity measurements and the numerical calculations along the axis of the mixing chamber in the presence of cells. The difficulty in making the hot-wire measurements and the limited number of grid points within the cell region (in the numerical results) may explain the differences between the two results. In addition, the artificial viscosity in the numerical calculations, particularly in the presence of large velocity gradients, and the observed unsteadiness of the downstream stagnation point may also account for part of the difference.

5) Both the smoke visualization and hot-wire results confirm Shavit and Lavan's[2,4] conclusion in reference to the weak dependence of the downstream stagnation point of the cell on the velocity ratio, λ, at a constant Reynolds number, Re.

References

[1] Wood, B., "Diffusion in Laminar Confined Jet," D. Sc. thesis, June 1964, MIT, Cambridge, Mass.

[2] Lavan, Z. and Shavit, G., "Recirculating Patterns in Confined Laminar Jet Mixing," *Israel Journal of Technology*, Vol. 9, Nos. 1-2, March 1971, pp. 51–60.

[3] Shavit, G. and Lavan, Z., "Analytical and Experimental Investigation of Laminar Mixing of Confined Heterogeneous Jets," AIAA Paper 71-601, Palo Alto, Calif., 1971.

[4] Shavit, G., "Analytical and Experimental Investigation of Laminar Mixing of Homogeneous and Heterogeneous Jets in a Confining Tube," Ph. D. thesis, June 1970, Illinois Inst. of Technology, Chicago, Ill.

[5] Rozenman, T. and Weinstein, H., "Recirculating Patterns in the Initial Region of Coaxial Jets," Paper 72-APM-30, San Diego, Calif., June 1972, ASME; also *Transactions of the ASME, Ser. E: Journal of Applied Mechanics*, to be published.

[6] Warpinski, N. R., Nagib, H. M. and Lavan, Z., "Experimental Investigation of Recirculating Cells in Laminar Coaxial Jets," AIAA Paper 72-150, San Diego, Calif., 1972.

[7] Comte-Bellot, G., Strohl, A., and Alcaraz, E., "On Aerodynamic Disturbances Caused by Single Hot-Wire Probes," *Transactions of the ASME, Ser. E: Journal of Applied Mechanics*, Vol. 38, No. 4, Dec. 1971, pp. 767–774.

[8] Roshko, A., "On the Development of Turbulent Wakes from Vortex Streets," Rept. 1191, 1954, NACA.

[9] Wygnanski, I. and Champagne, F., "On Transition in a Pipe," *23rd Physics of Fluids Annual Meeting of the American Physical Society, Bulletin of APS*, Ser. II, Vol. 16, No. 11, Nov. 1971, pp. 1323.

[10] Gebhart, B., *Heat Transfer*, 2nd ed., McGraw-Hill, New York, 1971, pp. 388–397.

[11] Collis, D. and Williams, M., "Two-Dimensional Convection from Heated Wires at Low Reynolds Numbers," *Journal of Fluid Mechanics*, Vol. 16, Pt. 3, Oct. 1959, pp. 357–384.

[12] Goodman, C., "Calibration of a Hot-Film Anemometer in Water Over the Velocity Range 0.5 to 200 cm/sec.," Ph. D. thesis, April 1971, Tulane Univ., New Orleans, La.

[13] Hollasch, K. and Gebhart, B., "Calibration of Constant-Temperature Hot-Wire Anemometers at Low Velocities in Water with Variable Fluid Temperature," *Transactions of the ASME, Ser. C: Journal of Heat Transfer*, Vol. 94, No. 1, Feb. 1972, pp. 17–22.

[14] Rasmussen, C. G., "The Air Jet Hot-Wire Microphone," DISA Information No. 2, July 1965, DISA S. & B. Franklin Lakes, New Jersey, pp. 5–13.

[15] Bhatt, K., "Study of Heat Transfer and Mixing in Laminar, Coaxial, Confined Streams," M.S. thesis, December 1970, Illinois Inst. of Technology, Chicago, Ill.